Bioorganic & Medicinal Chemistry 16 (2008) 9018–9022

Contents lists available at ScienceDirect

Bioorganic & Medicinal Chemistry

journal homepage: www.elsevier.com/locate/bmc

# Studies on inhibition mechanism of transcription factor NF-κB and DNA binding by chelator pyrogallol red on the basis of its interaction with metal ions

R. K. Sharma [a,*], C. Chelladurai [a], A. D. Tiwari [a], H. K. Rajor [a], S. Mehta [a], M. Otsuka [b]

[a] Green Chemistry Network Centre, Department of Chemistry, University of Delhi, Delhi 7, India
[b] Faculty of Medical and Pharmaceutical Sciences, Kumamoto University, 5-1 Oe-honmachi, Kumamoto 862-0973, Japan

ARTICLE INFO

*Article history:*
Received 16 March 2008
Revised 16 August 2008
Accepted 20 August 2008
Available online 26 August 2008

*Keywords:*
Pyrogallol red
Zinc
NF-κB–DNA binding
$^1$H NMR
IR
TGA and EMSA

ABSTRACT

Recent studies have shown that the zinc influences the DNA binding of transcription factor NF-κB. So the zinc-interaction of pyrogallol red (PR) an inhibitor of NF-κB–DNA binding was studied by isolating the zinc–PR complex. The complex was characterized using IR, UV–visible, $^1$H NMR, and thermal studies. Binding sites of PR were investigated by molecular modeling using MM+ and PM3 methods and by generating molecular electrostatic map. These studies have confirmed the role of metal ion chelation in the inhibition of NF-κB–DNA binding by PR.



## 1. Introduction

Nuclear factor-kappa B (NF-κB) is a Rel family transcription factor consisting of p50 and p65 subunits and sequestered in the cytoplasm by specific IκB proteins.[1–4] NF-κB can be activated by diverse stimuli such as microbial and viral products, proinflammatory cytokines, T- and B-cell mitogens, and physical, chemical, and oxidative stresses. Before activation, NF-κB/Rel dimers are bound to IκBs, and retained in an inactive form in the cytoplasm.[5–7] Following the activation, IκB is phosphorylated by IκB kinases,[8] polyubiquitinated by ubiquitin ligase complex,[9] and further degraded by the 26S proteasome. Finally NF-κB is released and translocated into the nucleus, where it binds to the target DNA (κB sites), and initiates gene expression. Recent studies have shown that the p50 subunit of the NF-κB complex is the one which mainly interacts with the HIV-1 LTR.[10–12] By binding to the κB sites, NF-κB mediates gene expression pathways, and is involved in a number of pathological events, including progression of AIDS by regulating the first step transcription and hence multiplication of human immunodeficiency virus type 1 (HIV-1).[13] Zinc plays an important role in the activation of NF-κB.[5] It has been reported that NF-κB inhibitory activity of compounds such as 1,10-phenanthroline[9] and aurintricarboxylic acid (ATA)[6] is related to their complex formation with zinc. In zinc-deficient cells, the activation of NF-κB is significantly decreased. Sharma et al. examined the effect of ATA on the DNA binding of NF-κB and found that ATA is the most potent inhibitor of NF-κB among the molecules tested so far[6] and demonstrated that ATA inhibited the NF-κB–DNA binding at a very low concentration and that the addition of zinc(II) partially restored the DNA binding resulting in replication of HIV virus.[7]

Studies with respect to recombinant NF-κB p50 binding to DNA suggest that NF-κB recognizes DNA by using zinc-dependent motifs. Zinc may also play a role in cross-linking the DNA binding of p50 dimer.[5] Therefore, the zinc-interaction of pyrogallol red (PR) (Fig. 1), an ATA analogue and NF-κB–DNA-binding inhibitor, was studied by isolating the zinc–PR complex. Binding sites of PR were identified by IR, UV–visible, $^1$H NMR, and thermal and molecular modeling studies.

## 2. Results and discussion

### 2.1. Physical properties of the complexes

The PR complex of zinc(II) has been isolated in methanol under normal conditions. The complex is dark blue in color. The complex is hygroscopic in nature and soluble in water, methanol, ethanol, and DMSO but insoluble in chloroform and carbon tetrachloride. On the basis of elemental analysis (Table 1), we found that PR acted as a bidentate ligand and formed a mononuclear complex in 1:1 ratio and the results suggest that the composition of complex is [Zn–PR·2$H_2O$].

* Corresponding author. Tel./fax: +91 11 27666250.
*E-mail addresses:* rksharmagreenchem@hotmail.com (R.K. Sharma), motsuka@gpo.kumamoto-u-ac.jp (M. Otsuka).

0968-0896/$ - see front matter © 2008 Elsevier Ltd. All rights reserved.
doi:10.1016/j.bmc.2008.08.038

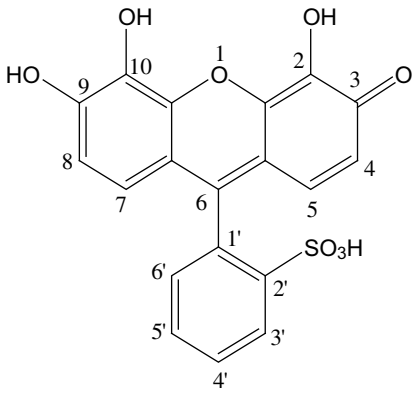


**Figure 1.** Pyrogallol red (PR).

**Table 1**
Elemental analysis of Zn–PR complex

| Complex | % Calculated (observed) | | | |
|---|---|---|---|---|
| | C | H | S | M |
| [Zn–PR] | 40.71(40.21) | 3.59(3.42) | 6.38(6.72) | 17.61 |

**Table 2**
UV–vis absorption spectral data of Zn–PR complex

| Ligand/complex | PR (nm) | Zn(II)–PR (nm) |
|---|---|---|
| Band I (MeOH) | 503 | 535 |
| Band II (MeOH) | 431 | 441 |

The absorption spectra of the PR and its zinc complex were recorded in methanol in the spectral range 300–800 nm. The characteristic absorption peaks with their assignment are given in Table 2. In the absorption spectra of free ligand two peaks at 503 nm (band I, phenolic system) and 431 nm (band II quinolic system) are observed[14] due to $\pi$–$\pi^*$ and $n$–$\pi^*$ transition. In the complex, the absorption spectrum of pyrogallol red is shifted to higher wavelength, that is, 535 nm and 441 nm. Such bathochromic shift can be explained by the extension of the conjugated system on complexation. The absorption band I was shifted more than band II, which indicates that band I is involved in coordination to the metal ion. These results suggest the involvement of 9-OH and 10-OH group in coordination with the metal ion.

## 2.2. IR spectra

The characteristic IR absorption frequencies in the spectral range 4000–400 $cm^{-1}$ were measured for metal-free PR and its zinc complex. The IR absorption frequencies of PR and its zinc complex are presented in Table 3. The IR spectrum of the Zn–PR complex clearly indicates that the free PR participates in coordination with the metal ion. In the ligand, the aromatic –OH shows two broad peaks at 3188 and 3401 $cm^{-1}$, while in the complex peak at 3188 $cm^{-1}$ disappears. In the ligand, C–O peak at 1588 $cm^{-1}$ is observed and in zinc complex it is shifted to lower frequency at 1576 $cm^{-1}$.[15,16] Single peak at 1372 $cm^{-1}$ in ligand for the skeletal vibration in a plane is shifted and splited into two broad peaks at 1397 $cm^{-1}$ in the complex spectrum, which shows that after coordination of zinc with PR the complex becomes nonplanar.

**Table 3**
IR absorption frequencies of Zn–PR complex

| Functional groups | PR ($cm^{-1}$) | Zn–PR ($cm^{-1}$) |
|---|---|---|
| $\nu$(O–H) | 3401 and 3188 | 3401 |
| $\nu$(C–H) | 2381 | 2387 |
| $\nu$(C=O) | 1653 | 1621 |
| $\nu$(C–O) | 1588 | 1576 |
| $\nu$(skeletal vibration in a plane) | 1372 | 1397 |
| C–O–H | 1108 | 1095 |
| $\nu$(aromatic ring out of plane) | 901 | 855 |

## 2.3. $^1$H NMR spectra

$^1$H NMR spectrum of the zinc complex was recorded in DMSO-$d_6$ solvent at 300 MHz. The data are summarized in Table 4. The resonance signals of coordinated PR are shifted downfield as well as upfield as compared to the free PR. It was observed that relative shift in the $^1$H NMR signal due to the deprotonation of OH in ligand when coordinated with zinc metal ion was not found in the spectra, because it is suppressed due to the DMSO-$d_6$ solvent. Resonance signal in Zn–PR complex, the adjacent CH proton is shifted upfield and other CH proton are shifted downfield and subjected to no perturbing influence other than the deshielding expected from the electron withdrawing inductive effect of coordination. Due to the coordination of PR with zinc metal ion, $^1$H NMR signal for CH($\alpha$) and CH($\beta$) is shifted upfield (6.96–6.86 ppm) and CH($\gamma$) and CH($\delta$) is shifted downfield (7.64–7.77 ppm).[17]

## 2.4. Thermal analysis

Thermogravimetric analysis of the complex was carried out to examine the thermal stability, number, and nature of the water molecule present in the complex. The thermogram was recorded in the temperature range 50–1000 °C in nitrogen atmosphere with heating rate 15 °C per minute and the data are shown in Table 5. The TGA curve shows that the first weight loss of the complex was 7.2%, observed between 150 and 180 °C, which corresponds to loss of two water molecules and second weight loss was 74.5% between the range of 220–800 °C corresponding to one molecule of PR. Therefore, composition of the complex is [Zn–PR·2$H_2O$].

## 2.5. Molecular modeling of Zn(II)–PR complex

The molecular geometry of the PR and its complex was optimized by molecular mechanics (MM+) and semiempirical method (PM3) using 'HyperChem' Professional version 7.51 software. To identify the binding site, net charges on each atom of PR have been assigned. In addition, MEP was generated from optimized minimum energy conformation of PR. Figures 2 and 3 show the energy minimized structure and MEP for the PR. Study of such potential map provides insight into the nature of molecular recognition in ligand–metal interaction.[18] The color-coded isosurface in Figure 3 represents positive potential in blue and a negative in red color. The better chelating sites are the ones, which have relatively more electronegative MEP surface.[19,20]

Energy minimized structure of Zn(II)–PR complex obtained by geometric optimization is shown in Figure 4. It was found that the probable chelating sites are 9- and 10-OH groups.

**Table 4**
$^1$H NMR chemical shift data (ppm) of Zn–PR complex in DMSO-$d_6$ on 300 MHz

| Compound | $H_4$–$H_8$(d) | $H_5$–$H_7$(d) | $H_2'$(d) | $H'_4$–$H'_5$(t) | $H_3'$(d) | $H_3'$(d) |
|---|---|---|---|---|---|---|
| PR | 6.96–6.93 | 7.35–7.33 | 7.31–7.29 | 7.64–7.63 | 7.71 | 8.05 |
| Zn–PR | 6.86–6.80 | 7.35–7.32 | 7.79–7.71 | 7.77–7.74 | 7.90 | 8.15 |

**Table 5**
Thermal analysis data of Zn–PR complex

| Complex | Temperature (°C) | % Weight loss | | Constituents eliminated |
|---|---|---|---|---|
| | | Calculated | Observed | |
| [Zn(PR)·2H$_2$O] | 50–120 | 7.20 | 7.01 | $H_2O$ |
| | 220–800 | 75.05 | 74.5 | One molecule of pyrogallol red |

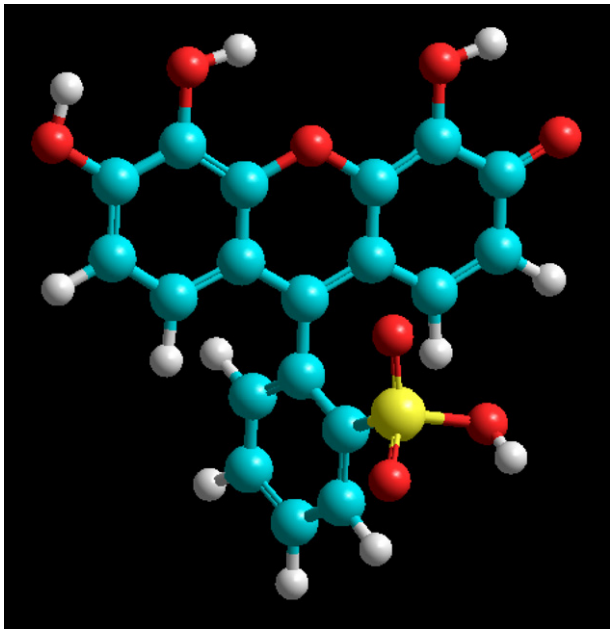

**Figure 2.** Energy minimized structure of PR by MM+ method $E$ = 40.4240, 0.096.

## 2.6. Electrophoretic nobility shift assay

PR shows the inhibitory effect on the DNA binding of $(p50)_2$ at 30 and 100 μM concentrations as demonstrated by EMSA (Fig. 5). It was carried out by using the chemiluminescence method, which offers the sensitivity and speed without producing hazardous radioactive waste. PR was found to exhibit remarkable inhibitory effects on the DNA binding of $(p50)_2$, both at 30 and 100 μM concentrations.[7] Several studies have demonstrated that zinc influences the DNA binding of NF-κB. Zabel et al.[9] have shown that the binding of NF-κB to DNA was specifically blocked by the chelating agent 1,10-phenanthroline and could be reconstituted only by the addition of zinc. Otsuka et al.[21] have examined the effects of four novel heterocyclic chelator compounds comprising (dimethylamino) pyridine and histidine units and their zinc complexes on NF-κB binding to DNA. Sharma et al.[6] demonstrated that ATA inhibited NF-κB–DNA binding at a very low concentration and that the addition of zinc(II) partially restored the DNA-binding property of NF-κB. Prasad et al.[5] have already suggested that NF-κB recognizes DNA by using zinc-dependent motifs. Zinc may play a role in cross-linking the DNA binding of the p50 dimer. Hence, the zinc-binding behavior of PR may be correlated with its ability to inhibit NF-κB–DNA binding.

## 2.7. Molecular modeling, docking studies

In an effort to rationalize the results obtained from EMSA studies, we resorted to the application of molecular modeling and computational methods with the intention of analyzing and reviewing the structure of the DNA-binding region (DBR) in complex with PR. Biochemical studies have hinted at a relationship between the structural conformation of p50 with its DNA-binding ability and function.[22] It is plausible that the compounds that have stronger interactions with important amino acid residues such as Ser66, His67, and Arg59 of the DBR of p50 would affect its conformation the most, thereby acting as good NF-κB–DNA-binding inhibitors. Considering this, PR was docked to the DBR (amino acid residues 59–71) of NF-κB (p50). The docked complex was refined with a progressive energy-minimization protocol using the AMBER force field. Figure 6 depicts the interaction of the PR with the p50-DNA-binding region after energy refinement. It is clear from this docked complex that PR, which is active, can form extensive hydrogen bonds with the DBR of p50. Theoretically calculated potentials, using ab initio methods, have been described to be very predictive.[23,24] PR has been found to form stronger complexes with zinc on the basis of its greater ability to complex with positively charged metal because of the presence of more electronegative potentials on its surface.

## 3. Conclusion

PR was shown to directly inhibit NF-κB–DNA binding. We have studied the metal chelation by using elemental analysis, UV–visi-

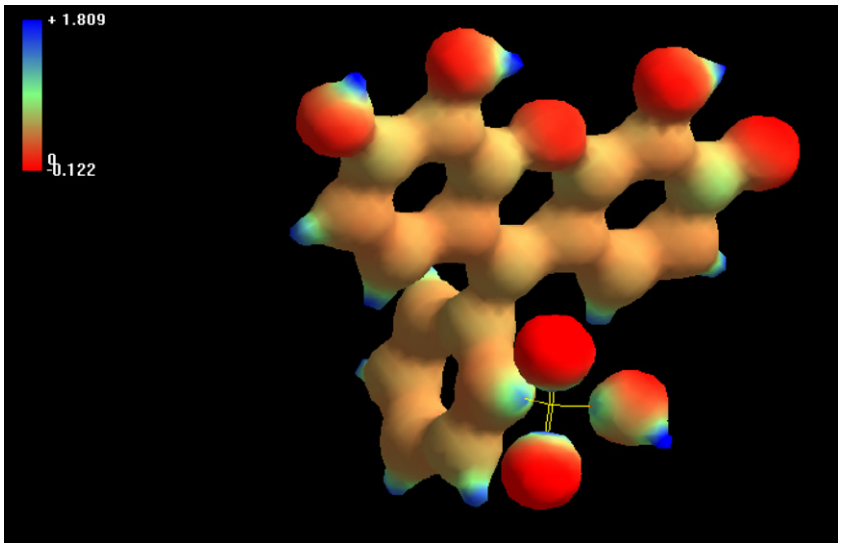


**Figure 3.** 3D Mapped isosurface molecular graph of PR electrostatic potential = minimum, −0.122; maximum, 1.809.

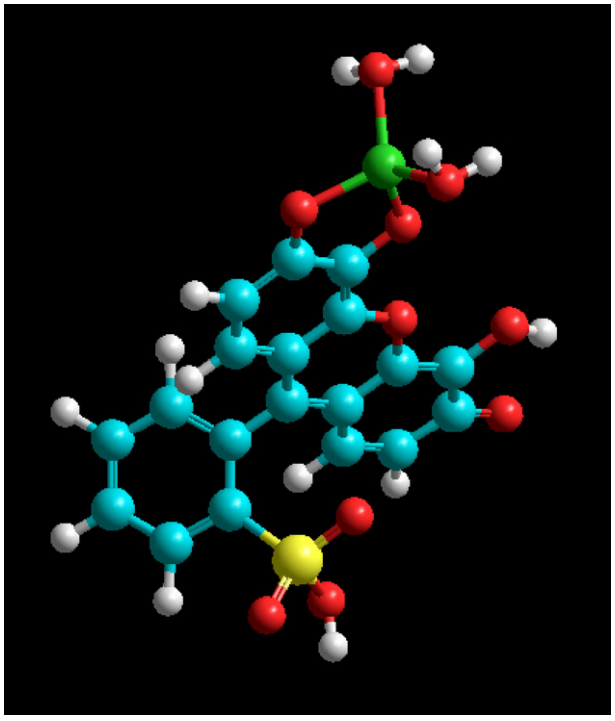

**Figure 4.** Energy minimized structure of Zn(II)–PR by using molecular mechanics, (MM+) $E$ = 51.1864, 0.0956.

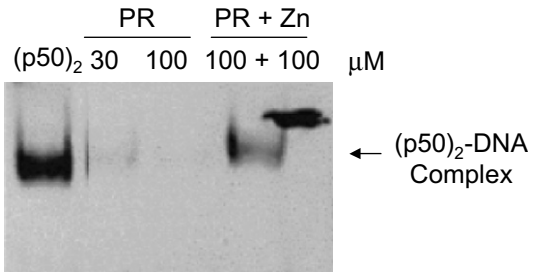


**Figure 5.** Effects of pyrogallol red (PR) on the DNA binding of $(p50)_2$. The effect of zinc on the inhibition of the DNA binding of $(p50)_2$ by PR is also shown.

ble, IR, and $^1$H NMR studies and found that zinc ion binding with PR through hydroxyl group at 9- and 10-positions. Thermogravimetric study shown that the complex losses two water molecules and one molecule of PR, which indicates that metal forms 1:1 complex with ligand. Molecular modeling studies supported the chelating sites predicted in the aforesaid studies. On the basis of above results structure of Zn–PR complex has been predicted and given in Figure 7. EMSA, molecular modeling, and docking studies gave the evidence in support of direct inhibition of NF-κB–DNA binding.

The present study concludes that the Zn–PR·$2H_2O$ complex formation plays very important role in inhibition of NF-κB–DNA binding.

## 4. Materials and methods

### 4.1. Reagents

All reagents and solvents were analytical reagent grade. Tetramethylammonium hydroxide, PR, and zinc acetate were procured from Merck, Acros Organics and Thomas Baker, respectively, and used as such in this study.

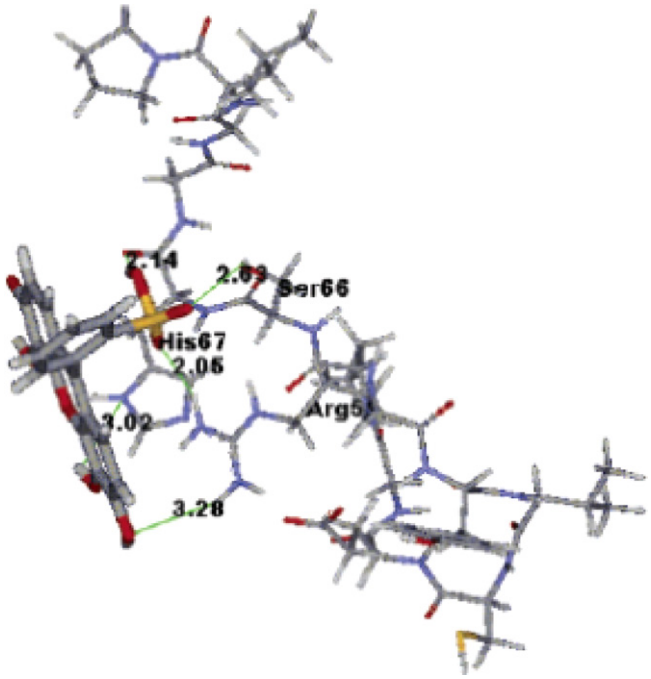


**Figure 6.** Possible binding modes of the PR with p50-DNA-binding region. Hydrogen bonds are depicted as green lines and distances are in Angstroms.

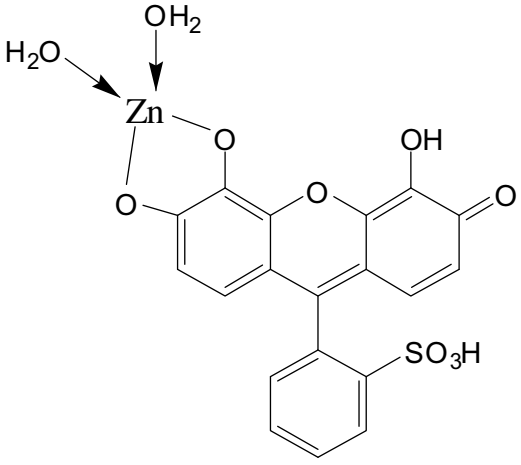


**Figure 7.** Tentative structure of Zn–PR complex.

### 4.2. Preparation of Zn(II)–PR complexes

Hot solution of PR (1 mM) in 50 mL methanol was added dropwise to the hot solution of 1 mM zinc acetate [$Zn(CH_3COO)_2{\cdot}2H_2O$] in 50 mL methanol. The reaction mixture was stirred thoroughly for 4 h at 50 °C temperature on hot plate, then it was refluxed for 8–12 h at 70 °C. The solution was left for slow evaporation at room temperature and after that dark blue color complex was collected from the solution and dried in vacuum desiccator over $P_4O_{10}$.

### 4.3. Instrumentation and measurement

Microanalysis (Carbon and Hydrogen) was carried out with a FISONS EA-1108 elemental analyzer. The thermogram was recorded on Du Pont TA 2000 TGA machine under nitrogen atmosphere at a heating rate of 15 °C $min^{-1}$. A Shimadzu UV-2501PC spectrophotometer was used to obtain the electronic spectra in

the region 300–800 nm in methanol. FTIR spectra in the 4000–400 $cm^{-1}$ regions were recorded from KBr pellets on a Perkin-Elmer FTIR Spectrophotometer 2000. $^1H$ NMR chemical shift was measured in DMSO-$d_6$ solvent on Bruker 300 MHz spectrometer.

### 4.4. Molecular modeling of the Zn(II)–PR complex

The molecular geometry of the PR was first optimized by molecular mechanics, MM+ and then by semiempirical method, PM3 using 'HyperChem' Professional version 7.51 Software.[25] To identify the binding sites, net charges on each atom on PR has been determined. In addition, molecular electrostatic map (MEP) of PR and its complex was generated.

### 4.5. Electrophoretic mobility shift assay

A biotinated double-stranded oligonucleotide containing a κB site from the mouse immunoglobulin κ light chain enhancer was used. Purified GST-p50 (5 ng) was used for the electrophoretic mobility shift assay (EMSA).

- 5′-Biotin-AGCTTCAGAGGGGACTTTCCGAGAGG-3′
- 3′-AGTCTCCCCTGAAAGGCTCTCCAGCT-Biotin-5′

After the incubation of reaction mixture containing the binding buffer (15 mM Tris–HCl (pH 7.5), 75 mM NaCl, 1.5 mM EDTA, 1.5 mM dithiothreitol, 7.5% glycerol, 0.3% NP-40, and 1 mg/mL BSA), 0.5 μg of polydI-dC, GST-p50, and PR at room temperature for 5 min, the labeled DNA probe (30,000 cpm) was added, and the mixture was further incubated at room temperature for 20 min. The sample in a volume of 10 μL was loaded onto 4% poly(acrylamide) gels and electrophoresed at 80 CV. After this, the gel was transferred to a nylon membrane. The biotin end-labeled DNA was detected using the streptavidin–horseradish peroxidase conjugate and lightshift chemiluminescent substrate.[26] This chemiluminescence assay method offers the sensitivity and speed of radioactive assays without the hazards, waste, and probe-instability problems associated with radioactive systems.

### 4.6. Molecular modeling, docking studies

The 3D structure of NF-κB (p50), obtained from the Protein Data Bank (pdb id: 1NFK)[27] was used to dock the PR. Docking studies were performed with the GOLD 2.0 program,[28] and the details of the docking procedure have been described in detail in our previous studies.[7] Briefly, the amino acid residues 59–71 (the DNA-binding region) in p50, which have been described to be very important in κB site specific DNA recognition,[26] were defined as the docking site. Docking simulations were performed in standard default settings to get the best predictive accuracy. GoldScore was used to rank the relative docking energies, and the highest scored solutions were considered. GoldScore[28] is a fitness function implemented in the GOLD program, which has four components: (a) protein–ligand hydrogen bond energy, (b) protein–ligand van der Waals energy, (c) ligand intramolecular hydrogen bond energy, and (d) ligand internal van der Waals energy. The Insight II molecular modeling package[29] was used for further analyses of the docked complexes.

## References and notes


1. Ghosh, S.; May, M. J.; Kopp, E. B. *Ann. Rev. Immunol.* **1998**, *16*, 225.
2. Siebenlist, U.; Franzoso, G.; Brown, K. *Ann. Rev. Cell Biol.* **1994**, *10*, 405.
3. Lander, H. M.; Ogiste, J. S.; Pearce, S. F.; Levi, R.; Novogrodsky, A. *J. Biol. Chem.* **1995**, *270*, 7071.
4. Scheinmann, R. I.; Cogswell, P. G.; Lofquist, A. K.; Baldwin, A. S. *Science* **1995**, *270*, 283.
5. Prasad, A. S.; Bao, B.; Beck, F. W. J.; Sarkar, F. H. J. *J. Lab. Clin. Med.* **2001**, *138*, 250.
6. Sharma, R. K.; Garg, B. S.; Kurosaki, H.; Goto, M.; Otsuka, M.; Yamamoto, T.; Inoue, J. *Bioorg. Med. Chem.* **2000**, *8*, 1819.
7. Sharma, R. K.; Chopra, S.; Sharma, S. D.; Pande, V.; Ramos, M. J.; Megaro, K.; Inoue, J.; Otsuka, M. *J. Med. Chem.* **2006**, *49*, 3596.
8. Brown, K.; Gerstberger, S.; Carlson, L.; Franzoso, G.; Siebenlist, U. *Science* **1995**, *267*, 1485.
9. Zabel, U.; Schreck, R.; Baeuerle, P. A. *J. Biol. Chem.* **1991**, *266*, 252.
10. Scherer, D. C.; Brockman, J. A.; Chen, Z.; Maniatis, T.; Ballard, D. W. *Proc. Natl. Acad. Sci. U.S.A.* **1995**, *92*, 11259.
11. Hiscott, J.; Kwon, H.; Genin, P. *J. Clin. Invest.* **2001**, *107*, 143.
12. Dickinson, L. A.; Trauger, J. W.; Baird, E. E.; Dervan, P. B.; Graves, B. J.; Gottesfeld, J. M. *J. Biol. Chem.* **1999**, *274*, 12765.
13. Yamamoto, Y.; Gaynor, R. B. *Curr. Mol. Med.* **2001**, *1*, 287.
14. Camilo, L.; López-Alarcón, C.; Lissi, E. *Free Radical Res.* **2005**, *39*, 729.
15. Coates, J. Interpretation of Infrared Spectra, A Practical Approach. In *Encyclopedia of Analytical. Chemistry*; Meyers, R. A., Ed.; John Wiley & Sons: Chichester, 2000; pp 10815–10837.
16. Nakamoto, K. *Infrared Spectra of Inorganic and Coordination Compounds*, 2nd ed.; John Wiley & Sons, 1969. p 308, Table 3.50.
17. Reddy, P. R.; Radhika, M.; Manjula, P. *J. Chem. Sci.* **2005**, *117*, 239.
18. *The Encyclopedia of Computational Chemistry*; Murray, J. S., Politzer, P., In Schleyer, P. V. R., Allinger, N. L., Clark, T., Gasteiger, J., Kollman, P. A., Schaefer, H. F., Schreimer, P. R., Eds.; Wiley and Sons: Chichester, UK, 1997.
19. Sharma, R. K.; Pande, V.; Ramos, M. J.; Rajor, H. K.; Chopra, S.; Meguro, K.; Inoue, J.; Otsuka, M. *Bioorg. Chem.* **2005**, *33*, 67.
20. Pande, V.; Sharma, R. K.; Otsuka, M.; Inoue, J.; Ramos, M. J. *J. Comput.-Aided Mol. Des.* **2003**, *17*, 825.
21. Otsuka, M.; Fujita, M.; Aoki, T.; Ishii, T.; Sugiura, Y.; Yamamoto, T.; Inoue, J. *J. Med. Chem.* **1995**, *38*, 3264.
22. Chen-Park, F. E.; Huang, D.-B.; Noro, B.; Thanos, D.; Ghosh, G. *J. Biol. Chem.* **2002**, *277*, 24701.
23. Sharma, R. K.; Otsuka, M.; Pande, V.; Inoue, J.; Ramos, M. J. *Bioorg. Med. Chem. Lett.* **2004**, *14*, 6123.
24. Yang, J. P.; Merin, J. P.; Nakano, T.; Kitade, Y.; Okamoto, T. *FEBS Lett.* **1995**, *361*, 89.
25. HyperChem version 7.51, Hypercube, Inc., USA.
26. Pierce Biotechnology, Inc., Rockford, IL.
27. Ghosh, G.; Van Duyne, G.; Ghosh, S.; Sigler, P. B. *Nature* **1995**, *373*, 303.
28. GOLD 2.0, CCDC software Ltd, Cambridge, UK.
29. INSIGHT II, Accelrys Inc., San Diego, CA.